Protein capped Cu nanoclusters-SWCNT nanocomposite as a novel candidate of high performance platform for organophosphates enzymeless biosensor

Hasan Bagheri, Abbas Afkhami, Hosein Khoshsafar, Ali Hajian, Alireza Shahriyari

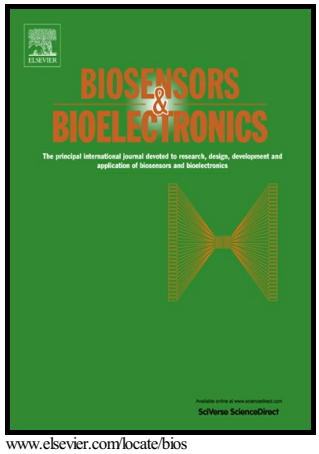

www.elsevier.com/locate/bios

PII: S0956-5663(16)30995-2
DOI: http://dx.doi.org/10.1016/j.bios.2016.10.003
Reference: BIOS9223

To appear in: *Biosensors and Bioelectronic*

Received date: 5 August 2016
Revised date: 28 September 2016
Accepted date: 3 October 2016

Cite this article as: Hasan Bagheri, Abbas Afkhami, Hosein Khoshsafar, Al Hajian and Alireza Shahriyari, Protein capped Cu nanoclusters-SWCNT nanocomposite as a novel candidate of high performance platform fo organophosphates enzymeless biosensor, *Biosensors and Bioelectronic* http://dx.doi.org/10.1016/j.bios.2016.10.003

Protein capped Cu nanoclusters-SWCNT nanocomposite as a novel candidate of high performance platform for organophosphates enzymeless biosensor

Hasan Bagheri [a,*], Abbas Afkhami [b], Hosein Khoshsafar [b], Ali Hajian [c], Alireza Shahriyari [a]

[a] *Chemical Injuries Research Center, Baqiyatallah University of Medical Sciences, Tehran, Iran*

[b] *Faculty of Chemistry, Bu-Ali Sina University, Hamedan, Iran*

[c] *Laboratory for Sensors, Department of Microsystems Engineering (IMTEK), University of Freiburg, Georges Köhler Allee 103, 79110 Freiburg, Germany*

Corresponding author. Tel./fax: +9821 82842368.
E-mail address: h.bagheri@bmsu.ac.ir; h.bagheri82@gmail.com (H. Bagheri).

Abstract

A biocompatible nanocomposite including bovine serum albumin (BSA) template Cu nanoclusters (CuNCs@BSA) and single-walled carbon nanotubes (SWCNT) was synthesized to fabricate a highly sensitive electrochemical biosensor for paraoxon as a model of organophosphates. The UV-Vis, fluorescence and Fourier transform infrared (FTIR) demonstrated that BSA entrapped in the nanocomposite film have been changed in its secondary structure so that it provided an enzyme like activity attributing to the high electrical conductivity of the entrapped copper nanoclusters. Also, the morphology and structure of prepared nanocomposites were investigated by transmission electronic microscopy (TEM) and scanning electron microscopy (SEM). In the prepared nanocomposite, the CuNCs@BSA found to play as

a conductive holder as well as an accumulator of redox active centers on the surface of the electrode, and SWCNT improves the electrocatalytic activity along with conductivity of glassy carbon electrode (GCE) surface. The fabricated biosensor exhibited excellent sensitivity, acceptable stability, fast response, and high electrocatalytic activity toward the reduction of paraoxon. The reduction peak current *vs* paraoxon concentration was linear over the range 50 nM to 0.5 μM and 0.5 to 35 μM, with a limit of detection of 12.8 nM. Notable electrocatalytic properties of the developed electrode toward paraoxon indicated that the nanocomposite possesses a promising potential to fabricate the third generation enzyme-free electrochemical biosensors, bioelectronics and state-of-the-art biomedical devices in the future.

Keywords: Enzymeless biosensor; Electrochemical biosensors; Paraoxon; Cu nanoclusters; Organophosphorus; SWCNT.

1. Introduction

Pesticides which can be divided to fungicides, insecticides and herbicides are widely used in agriculture to control hazardous micro-organisms, increase yield, and subsequently reduce the cost of food production (Tiwari et al. 2015). However, long-term and widespread usage of pesticides, caused severe contamination of soil, water, air, and agricultural products, finally being destructiveness to the ecosystems including animals and humans. Owning to easily degradable, highly effective in pest control, and less accumulation in living body, organophosphates (Ops) including paraoxon and parathion are major pesticides which are routinely used (Qian and Lin 2015). Nonetheless, OPs exhibit acute toxicity to animal and human health through their residues in contaminated water and agricultural products which result

in a deleterious effect on the visual, nervous, respiratory and cardiovascular system and even death (Dong et al. 2015; Zhang et al. 2014). Therefore, developing an accurate, sensitive, rapid, and simple method for detection of OPs is urgent demand in human health regarding the concerns of the human safety and environmental protection.

Many conventional techniques such as gas chromatography-mass spectrometry (GC-MS) (Gómez-Ramos et al. 2013), high performance liquid chromatography (HPLC) (Wang et al. 2012), spectrophotometry (Hu et al. 2010), flow injection analysis (Dominguez et al. 2015), and capillary electrophoresis (Tang et al. 2016) have been used for effective measurement of the OPs in food and environment. Even though these methods exhibit adequate selectivity and sensitivity, they are expensive, required multiple steps, and skilled manpower, which makes them be impractical for the regular and on-site environment and food safety monitoring. Recently, numerous enzyme-modified Ops biosensors with low detection limit, and high sensitivity have been developed based on activity inhibition of the acetylcholinesterase (AChE) and butyrylcholinesterase (BChE) activity or Ops hydrolysis by organophosphorus hydrolase (OPH) (Arduini et al. 2015; Songa and Okonkwo 2016; Yu et al. 2015; Zhao et al. 2015). However, the most common and serious problem is the enzyme stability and activity which can be easily affected by pH, temperature, and humidity, also a complicated and multi-step procedure, including cross-linking, adsorption, electropolymerization, and entrapment, which may decrease the enzyme activity is required to immobilize the enzyme on the electrode (Amine et al. 2016). Furthermore, most of them are required to deoxygenization or Ops detection which is inconvenient for on-site monitoring. To address these issues, it is necessary to develop an enzyme free electrochemical sensor for the detection of OPs because of their simplicity, stability, inexpensively, and capability for on-site detection. To the best of our knowledge, there are only a

few reports about enzymeless electrochemical sensor for Ops detection in recent years (Dong et al. 2015; Zhang et al. 2014; Singh 2016). Therefore, the enzyme-free Ops sensor is an attractive alternative tool.

Metal nanoclusters (NC) with a size range of a few nanometer, typically consist of several to tens of atoms. Their properties are governed by their subnanometer dimensions (Xie et al. 2009). This size regime is comparable to the Fermi wavelength of the conduction electrons. They have exhibited promising potential in a wide range of applications such as nanodevice, optoelectronic, nanoelectronic, novel catalysts, and sensing, because of their ultra-small size and spatial confinement of free electron in them (Lu and Chen 2012; Tiwari et al. 2013; Xie et al. 2009; Wen et al. 2013). Biomacromolecules provide a green chemistry protocol for the preparation of metallic NCs which not only will increase their biocompatibility but also will provide a surface with many functional groups. Among all the biomacromolecules, proteins, peptides, and DNA are commonly used in templating the synthesis of NCs (Shamsipur et al. 2016; Shang et al. 2011). BSA, the most abundant plasma protein, as a multifunctional and soft protein widely used in applications such as sensing, self-assembly, and imaging, was selected as the model protein for the synthesis of NCs. It shows a strong affinity towards inorganic salts, thus is widely used as biotemplate of metal NCs (Tao et al. 2015; Xie et al. 2009). Furthermore, the protein-capped metal NCs with good conductivity have successfully shown a promising potential as electrochemical interfaces for sensitive detection of glucose, H_2O_2, KB cells, tumor markers, and retinal-binding protein (Hu et al. 2013a; Hu et al. 2013b; Hu et al. 2012; Hu et al. 2014; Shamsipur et al. 2015).

Carbon nanotubes (CNTs) based nanocomposites have shown numerous applications to improve the host material properties, especially in the areas of biosensing and catalysis

(Chinnappan et al. 2016). For instance, enhanced catalytic activity has been demonstrated in the nanocomposites of Pd-Pt-CNT (Yang et al. 2016), MnO_2-CNT (Begum et al. 2016), CuS-CNT (Zhang et al. 2016) and TiN-CNT (Haldorai et al. 2016). Owing to the large surface area as well as high electron transport capability of CNTs, they are ideal materials to load more catalysts, ensuring high contact between the host materials CNT and ease fast electron transport. Considering the unique properties, it is reasonable to expect that CuNCs@BSA-SWCNT nanocomposite, which can be readily synthesized by taking advantage of the strong π-π stacking interaction between hydrophobic bases of the capped protein and SWCNT, may provide a sensitive knob to tune the properties and improve the catalytic activity.

In order to fabricate an enzymeless biosensor for Ops, we used a green and simple strategy to synthesize a protein-capped CuNCs with good sensing properties. Besides the good biocompatibility and considerable environmental/cost advantages of this methodology, the BSA coating layer on CuNCs also facilitated post-synthesis surface modifications with functional materials. Then, SWCNTs have been utilized to improve the electrocatalytic activity of as-prepared NC. To the best of our knowledge, this is the first time that the direct electrochemistry of protein template CuNCs and their high electrocatalytic property towards Ops sensing has been studied. The fabricated biosensor exhibited excellent sensitivity, acceptable stability, fast response, and high electrocatalytic activity toward the reduction of paraoxon.

2. Experimental

2.1. Chemicals and instrumentation

This section is described in detail in the supplementary information.

2.2. Synthesis of CuNCs@BSA and CuNCs@BSA-SWCNT

In a typical procedure, an aqueous solution of $Cu(NO_3)_2$ (10 ml, 5 mM) was added to BSA solution (10 mL, 20 mg/mL) under continuous stirring at room temperature. After 2-3 min, we used 1.0 M NaOH solution to adjust pH to the desired value (pH=12). Finally, we allowed the mixture to stir for 6-8 hours at 37 ^{0}C during which the color gradually changed to light brown (Goswami et al. 2011). After that the solution was dialyzed against phosphate buffer solution (PBS) using a dialysis tubing (MWCO 10 kD) for 72 h to remove all the free Cu ions from the solution and then freeze-dried to obtain a solid powder for subsequent characterization and investigations. For the synthesis of CuNCs@BSA-SWCNT nanocomposite, the 0.2 mg of SWCNT were added to 5 ml of CuNCs@BSA, kept sonicating for 30 min, and then centrifuged. The resulting participate was desired nanocomposite (Scheme 1).

2.3. Preparation of electrochemical biosensor

A GCE was polished to a mirror-like surface with 0.3 and 0.05 mm aluminum slurry, respectively. Subsequently, the electrode was rinsed with 1:1 HNO_3-H_2O (v/v), ethanol and doubly distilled water in an ultrasonic bath for 2-3 min for each wash and dried under nitrogen at room temperature. Then, the biosensor based on CuNCs@BSA-SWCNT composite was prepared with the following simple procedure: 10 μl of the as-prepared composite was cast on the surface of GCE and the electrode was dried in air (Scheme 1).

3. Results and Discussion

3.1. Characterization of CuNCs@BSA and CuNCs@BSA-SWCNT nanocomposites

BSA is a strong candidate for the synthesis of nanoclusters because it contains a large number of cysteine, tyrosine, and charged residues and has a known propensity to bind to metal ion complexes and functional groups of BSA (–COOH,–NH and –SH) provide a suitable sites for interaction target analyte (Xu et al. 2014; Hu et al. 2013a; Hu et al. 2013b; Hu et al. 2012).

Furthermore, the 3D complexed structures of BSA can withstand a wide range of pH and can be easily conjugated with other systems. The protein are expected to influence the nanocluster formation and property because of the diversity in amino acid contents and sequences (Xu et al. 2014). The characterizations of synthesized CuNCs@BSA and CuNCs@BSA-SWCNT nanocomposites were done using different methods. The pure BSA solution was pale yellow in color under visible light and emitted a weak blue fluorescence under UV light which was characteristic of the aromatic side groups in the amino acid residues (tryptophan, tyrosine and phenylalanine). In the UV-Vis spectra (Fig. 1a) the decrease in absorption peak related to aromatic residues of amino acids at 280 nm in CuNCs@BSA compared to BSA solution can be due to the formation of NC (Goswami et al. 2011). Furthermore, the intense fluorescence peak (λ_{exc}: 325 and λ_{emi}: 420 nm) confirmed the formation of CuNCs@BSA (Fig. 1b). Also, the SWCNT did not exhibit characteristic peak (Yuan et al. 2013). However, by synthesis of CuNCs@BSA-SWCNT the emission band of the fluorescence spectrum of CuNCs@BSA has been quenched (Figs. 1a and b), which can be due to strong interaction along with energy and electron transfer contribution between SWCNT and CuNCs@BSA to form nanocomposite (Shang and Dong 2008). We also employed the FTIR spectroscopy to study the synthesis process. By comparing the IR spectra of NCs and the free BSA and SWCNT, one can study the formation mechanism of NCs. As Fig. 1c reveals, there were O–H, N–H, C–N, and C=O groups on the surface of the CuNCs@BSA. The IR spectra of SWCNT showed the existence of two obvious absorption bands at about 1700 and 3400 cm^{-1}. The former can be assigned to characteristic of C=O stretches and the latter is identified as O–H stretching mode in carboxylic acid groups. Also, CuNCs@BSA-SWCNT showed a shift in the bands of amide I and II regions indicating a slight change of the secondary structure of the pure BSA protein. The results exhibit

partial unfolding of the protein in the presence of NCs which can be due to binding of Cu ions or atoms to such functional groups of the protein residues as -NH_2 and -COOH (Le Guével et al. 2011; Xu et al. 2014; Greenfield 2006).

Images of the products by SEM confirmed the successful synthesis of CuNCs@BSA-SWCNT nanocomposite. According to Fig. 1d, CuNCs@BSA is an agglomeration of nanoclusters. It is interesting to note that the smaller nanoclusters tend to have spherical shapes and appear to have fused slightly with their adjacent nanoclusters. SWCNT with a relative regular distribution with special three-dimensional structure were observed in SEM image of the SWCNT. The average diameter of the SWCNT seems to be varied in the range of 15-40 nm. In CuNCs-SWCNT the CuNCs partially decorating the SWCNT sidewalls form isolated nanoclusters partially interconnected, while the CuNCs@BSA decorating SWCNT sidewalls in continuous manner and nanoclusters merge together to form larger nanoclusters. According to Fig. 1d, the clusters are tightly attached to the SWCNT and formed well in nanocomposite structure. Morphology of CuNCs@BSA was investigated by TEM. TEM image of the CuNCs@BSA sample exhibits NCs with narrow size distribution and spherical morphology (Fig. 1d). Based on the results we conclude the nanocomposite is successfully synthesized.

3.2. Electrochemical characterization of biosensor

Electrochemical impedance spectroscopy (EIS) has been commonly used to probe the electrode surface change during stepwise assembly process (Barsoukov and Macdonald 2005; Bagheri et al., 2016a). In EIS the semicircular part at higher frequencies and linear part at lower frequencies correspond to the electron transfer resistance (R_{ct}) and the diffusion limited process, respectively. The diameter of semicircle equals R_{ct}, which reflects the interfacial electron transfer ability and electron transfer kinetic of redox probe (Bard et al. 1980; Bagheri et al., 2015; Shin et

al. 2016). Figure 2a showed the R_{ct} values of the bare and modified electrodes in the presence of redox probe. As can be seen, bare GCE after electrochemical pretreatment exhibited a small R_{ct} value of 185 Ω (blue curve). The CuNCs-SWCNT/GCE revealed a very small semicircle domain (R_{ct} = 62 Ω), implying a very low electron-transfer resistance of the redox probe showing that the SWCNT promoted conductivity. Then, GCE surface was modified with CuNCs@BSA-SWCNT nanocomposite to form a 3D layer. With the successful assembly of CuNCs@BSA-SWCNT, the R_{ct} value decreased to 107.5 Ω, indicating the accelerated electron transfer rate than GCE which can be due to nature of CuNCs and presence of SWCNT. The R_{ct} value of CuNCs@BSA-SWCNT increased with assemble of BSA. We supposed that a large amount of BSA was immobilized on the binding sites in the CuNCs (Afkhami et al., 2016)

In order to obtain the electrochemical active surface areas of GCE, CuNCs-SWCNT/GCE and CuNCs@BSA-SWCNT, the cyclic voltammetry of potassium ferrocyanide was performed using the Randles-Sevcik equation (1):

$$I_p = (2.69 \times 10^5)n^{3/2}AC^*D^{1/2}v^{1/2} \quad (1)$$

where I_p refers to the anodic peak current, n is the total number of electrons transferred (n = 1), A is the effective surface area of the electrode, D is the diffusion coefficient for $K_4[Fe(CN)_6]$ =7.6 $\times 10^{-6}$ cm^2 S^{-1}, C* is the concentration of $K_4[Fe(CN)_6]$ and *v* is the scan rate (Fig. 2bI) (Bagheri et al. 2016b). The surface area of CuNCs@BSA-SWCNT/GCE (0.247 cm^2) is higher than the CuNCs-SWCNT/GCE (0.218 cm^2) and GCE (0.068 cm^2). The increase of the electroactive surface area of the modified electrode showed the influence of CuNCs@BSA-SWCNT as an effective platform that provides a large surface and facilitates the electron transfer between the electrode and the solution.

Also, electrochemical behaviors of different fabricated electrodes were recorded in $Fe(CN)_6^{3-/4-}$ and KCl solution using CV (Fig. 2b II). On Bare GCE, a pair of weak redox peaks with the peak-to-peak separation (ΔE_p) of 0.24 V was observed, indicating the sluggish electron transfer rate at the interface. On the CuNCs-SWCNT/GCE, a pair of well-defined peaks appeared with lower ΔE_p value which was due to the synergic effects between CuNCs and SWCNT then the conductivity of the whole electrode surface was further improved. On the CuNCs@BSA-SWCNT/GCE, the symmetric redox peaks and lower peak currents than that on CuNCs-SWCNT/GCE were obtained, indicating that the surface conductivity and reaction reversibility of electrode were suitable by the presence of CuNCs@BSA-SWCNT.

3.3. Electrocatalytic activity of fabricated biosensor and electrochemical behavior of OPs

Figure 2c shows the CVs of bare GCE, CuNCs@BSA/GCE, SWCNT/GCE, and CuNCs@BSA-SWCNT/GCE in PBS before (2cI) and after (2cII) the addition of 100 μM paraoxon, respectively. As seen, no redox peaks were observed for the CVs at either bare or modified GCE in the absence of paraoxon, indicating the high electrochemical stability of CuNCs@BSA and CuNCs@BSA-SWCNT over a wide potential window. However, in the presence of paraoxon an irreversible cathodic peak at -0.55 V corresponding to the of nitryl ($-NO_2$) group of paraoxon was observed for the CuNCs@BSA/GCE as well a reversible peak at approximately -0.12 V corresponding to the conversion between hydroxyamino (-NHOH) and nitroso group (-NO) electrochemically reduced from nitryl (Zhang et al. 2014). The voltammograms of CuNCs@BSA-SWCNT/GCE showed an obvious increase in the two redox peaks. The irreversible peak involved the reduction of nitryl into hydroxyamino in the four-electron and four-proton transfer process (Scheme 1). Similarity, the reversible redox peaks can be attributed to the conversion of the hydroxyamino group to a nitroso group via a two-electron

and two-proton transfer process (Scheme 1). Because no significant catalytic peak for the paraoxon was observed at the bare GCE or at the SWCNT/GCE in this potential range, the high catalytic activity of CuNCs as well as the enhanced catalytic activity of SWCNT towards the electrochemical reduction of paraoxon to a great extent was concluded.

3.4. Parameters Optimization

In the following sections, the experimental conditions such as buffer pH, preconcentration potential and time were investigated for the peak current (-0.12 V) to improve the detection sensitivity of paraoxon at the fabricated electrode.

Because of participation of proton in the electrocatalytic reaction at CuNCs@BSA-SWCNT/GCE, the pH solution has a significant effect on the sensitive detection of Ops. As is shown in Figs. 3a and b, the peak potentials have negatively shifted in the pH range of 4.0-8.0 and the maximum peak current and best peak shape obtained at pH 6.0. In fact, this pH value is the most suitable condition because the hydroxyamino is produced and reduced to nitryl (Scheme 1, mechanism), which causes to have the best SWV response. So, a PBS buffer of pH 6.0 was selected for further studies.

The effects of preconcentration potential (PP) and time (PT) on the peak current response are exhibited in Fig. 3b. By changing the PP from 0 to -1.0 V, the cathodic peak current increased and the maximum plateau was reached at -0.8 V. Therefore, -0.8 V was chosen as the optimum PP for sensitive detection of paraoxon. Then, the PT as another effective parameter was optimized. As can be seen in the Fig. 3b the PT was increased, when the peak current increased and reached a maximum at about 180 s, and then remained unchanged. So, the optimized PP and PT were -0.8V and 180 s, respectively.

3.5. Analytical performance of the biosensor

Under optimum conditions, SWV signals proportionally increased by increasing the concentration of paraoxon at the CuNCs@BSA-SWCNT/GCE (Fig. 3c). The plot of response current *vs* paraoxon concentration was linear over the concentration range 50 nM to 0.5 μM and 0.5 to 35 μM, with linear regression equations I_{pc}(μA)=3.6117 C(μM)+0.6373 (R^2=0.994) and I_{pc}(μA)=0.6405 C(μM) +4.6104 (R^2= 0.996), respectively (Fig. 3d). The limit of detection (LOD) of the developed biosensor was 12.8 nM based on signal-to-noise ratio between 3 or 2:1. Determination of the signal-to-noise ratio is performed by comparing measured signals from samples with known low concentrations of analyte with those of blank samples and establishing the minimum concentration at which the analyte can be reliably detected. It is obvious that the designed biosensor shows excellent sensitivity along with wide linear range, and possessing a promising potential to be one of the most generally analytical methods used for determining of very low concentration of paraoxon.

Repeatability and reproducibility CuNCs@BSA-SWCNT/GCE were investigated by SWV measurements of 10 μM paraoxon in 0.1 M PBS buffer at pH 6.0. For five consecutive scans on the same electrode, the relative standard deviation (RSD) was 4.12% which shows good repeatability of the developed biosensor. Also, the SWV response of five identically modified CuNCs@BSA-SWCNT/GCE electrode exhibit an RSD of 4.85% confirming the acceptable reproducibility of the system. Moreover, nearly 96% of the initial SWV response of modified electrode was remained after 5 days storage demonstrating acceptable stability. The results verify that the biosensor has good repeatability, reproducibility, and stability toward paraoxon detection. Also, from the viewpoints of simplicity, sensitivity, wide linear range, low LOD, acceptable stability and very fast response, the proposed biosensor can be ranked as an effective reported paraoxon sensors (Table 1).

The response of the fabricated sensor toward paraoxon was also evaluated in the presence of some common species found in real samples. The results revealed that 400-fold of glucose, sucrose, fructose, alanine and glycine did not affect the selectivity. It was found that 200-fold of SO_4^{2-}, Cl^-, F^-, Ca^{2+} , Mg^{2+}, Li^+, Na^+, K^+ have no influence on the signal of paraoxon. Moreover, the responses of paraoxon in the presence of sevin, simazine, sutan, diazinon and atrazine were examined. It was found that same concentration of these compounds had no effect on the response of paraoxon. Interestingly, the presence of oxygen has a significant effect on the Ops detection because of the nitryl and oxygen reduction potential similarity. However, in this study, the oxygen presence does not have a considerable effect on paraoxon detection because the reduction peak (at -0.12 V) of the intermediate products was investigated instead of nitryl reduction peak for the p-nitrophenyl detection.

3.6. Real Sample analysis

We used the river, waste, and well water samples to investigate the capability of CuNCs@BSA-SWCNT/GCE in practical applications. After filtering the water samples to remove large particles, the pH was adjusted to 6.0. Table 2 presented the SWV response to spike different concentration of paraoxon to the water samples, in which the recoveries of spiked paraoxon in real samples were observed in the range from 93% ± 4% to 104% ± 3%. The results indicate the high reliability of the proposed biosensor. Moreover, the investigation confirms that the matrix effects from real water samples have not interference with the detection of OPs, demonstrating its high selectivity against naturally occurring compounds in real water samples.

4. Conclusion

To date, most of the paraoxon sensor are enzyme based, which may have very low LOD. However, they suffer from complicated and multi-step procedure along with the sensitivity of the

enzyme to the temperature, humidity, pH and sample matrix. In this work, we have developed a facile and eco-friendly strategy for the synthesis of CuNCs@BSA-SWCNT nanocomposites. Direct electrochemistry of protein capped CuNCs@BSA was investigated when the protein templated copper NCs were used to the synthesis of CuNCs@BSA-SWCNT nanocomposite immobilized on a GCE for detecting of paraoxon as the model of OPs. To the best of our knowledge, this is the first time that the direct electrochemistry of protein template copper nanoclusters and their high electrocatalytic property towards Ops sensing has been studied. The CuNCs@BSA play a role as a conductive holder as well as an accumulator of redox active centers on the surface of GCE and SWCNT improved the electrocatalytic activity along with conductivity of the surface. Notable electrocatalytic properties of CuNCs@BSA-SWCNT as a non-enzymatic electrochemical biosensor in this study offering the proposed nanocomposite as a candidate to fabricate the third generation enzymeless electrochemical biosensors, bioelectronics, biocatalysis as well as state-of-the-art biomedical devices in the future.

Acknowledgment:

The authors gratefully acknowledge the Dr Y. Hoseinzadeh Ardakani and Dr Afkhami laboratories for the instrumental support. Also, we acknowledge from the Research Council of Baqiyatallah University of Medical Sciences.

Supporting information. Supplementary data Supplementary material related to this article can be found, in the online version.

References:

Afkhami, A., Hashemi, P., Bagheri, H., Salimian, J., Ahmadi, A., Madrakian, T., 2016. Impedimetric immunosensor for the label-free and direct detection of botulinum neurotoxin serotype A using Au nanoparticles/graphene-chitosan composite. Biosensors and Bioelectronics, DOI: 10.1016/j.bios.2016.09.059.

Amine, A., Arduini, F., Moscone, D., Palleschi, G., 2016. Recent advances in biosensors based on enzyme inhibition. Biosensors and Bioelectronics 76, 180-194.
Arduini, F., Forchielli, M., Amine, A., Neagu, D., Cacciotti, I., Nanni, F., Moscone, D., Palleschi, G., 2015. Screen-printed biosensor modified with carbon black nanoparticles for the determination of paraoxon based on the inhibition of butyrylcholinesterase. Microchimica Acta 182(3-4), 643-651.
Bagheri, H., Ranjbari, E., Amiri-Aref, M., Hajian, A., Hosseinzadeh Ardakani, Y., Amidi, S., 2016a. Modified fractal iron oxide magnetic nanostructure: A novel and high performance platform for redox protein immobilization, direct electrochemistry and bioelectrocatalysis application. Biosensors and Bioelectronics 85, 814-821.
Bagheri, H., Khoshsafar, H., Afkhami, A., Amidi, S., 2016b. Sensitive and simple simultaneous determination of morphine and codeine using a Zn_2SnO_4 nanoparticle/graphene composite modified electrochemical sensor. New Journal of Chemistry 40, 7102-7112.
Bagheri, H., Talemi, R.P., Afkhami, A., 2015. Gold nanoparticles deposited on fluorine-doped tin oxide surface as an effective platform for fabricating a highly sensitive and specific digoxin aptasensor. RSC Advances 5, 58491-58498.
Bard, A.J., Faulkner, L.R., Leddy, J., Zoski, C.G., 1980. Electrochemical methods: fundamentals and applications. Wiley New York.
Barsoukov, E., Macdonald, J.R., 2005. Impedance spectroscopy: theory, experiment, and applications. John Wiley & Sons.
Begum, H., Ahmed, M.S., Jeon, S., 2016. A novel δ-MnO 2 with carbon nanotubes nanocomposite as an enzyme-free sensor for hydrogen peroxide electrosensing. RSC Advances 6(56), 50572-50580.
Chinnappan, A., Baskar, C., Kim, H., Ramakrishna, S., 2016. Carbon nanotube hybrid nanostructures: future generation conducting materials. Journal of Materials Chemistry A. 4, 9347-9361
Choi, B.G., Park, H., Park, T.J., Yang, M.H., Kim, J.S., Jang, S.-Y., Heo, N.S., Lee, S.Y., Kong, J., Hong, W.H., 2010. Solution chemistry of self-assembled graphene nanohybrids for high-performance flexible biosensors. ACS nano 4 (5), 2910-2918.
Dominguez, R.B., Alonso, G.A., Muñoz, R., Hayat, A., Marty, J.-L., 2015. Design of a novel magnetic particles based electrochemical biosensor for organophosphate insecticide detection in flow injection analysis. Sensors and Actuators B: Chemical 208, 491-496.
Dong, J., Hou, J., Jiang, J., Ai, S., 2015. Innovative approach for the electrochemical detection of non-electroactive organophosphorus pesticides using oxime as electroactive probe. Analytica Chimica Acta 885, 92-97.
Gómez-Ramos, M., Ferrer, C., Malato, O., Agüera, A., Fernández-Alba, A., 2013. Liquid chromatography-high-resolution mass spectrometry for pesticide residue analysis in fruit and vegetables: screening and quantitative studies. Journal of Chromatography A 1287, 24-37.
Goswami, N., Giri, A., Bootharaju, M., Xavier, P.L., Pradeep, T., Pal, S.K., 2011. Copper quantum clusters in protein matrix: potential sensor of Pb^{2+} ion. Analytical Chemistry 83(24), 9676-9680.
Greenfield, N.J., 2006. Using circular dichroism spectra to estimate protein secondary structure. Nature protocols 1(6), 2876-2890.
Haldorai, Y., Hwang, S.-K., Gopalan, A.-I., Huh, Y.S., Han, Y.-K., Voit, W., Sai-Anand, G., Lee, K.-P., 2016. Direct electrochemistry of cytochrome c immobilized on titanium nitride/multi-

walled carbon nanotube composite for amperometric nitrite biosensor. Biosensors and Bioelectronics 79, 543-552.
Hu, C., Yang, D.-P., Wang, Z., Huang, P., Wang, X., Chen, D., Cui, D., Yang, M., Jia, N., 2013a. Bio-mimetically synthesized Ag@ BSA microspheres as a novel electrochemical biosensing interface for sensitive detection of tumor cells. Biosensors and Bioelectronics 41, 656-662.
Hu, C., Yang, D.-P., Wang, Z., Yu, L., Zhang, J., Jia, N., 2013b. Improved EIS performance of an electrochemical cytosensor using three-dimensional architecture Au@ BSA as sensing layer. Analytical Chemistry 85(10), 5200-5206.
Hu, C., Yang, D.-P., Xu, K., Cao, H., Wu, B., Cui, D., Jia, N., 2012. Ag@ BSA core/shell microspheres as an electrochemical interface for sensitive detection of urinary retinal-binding protein. Analytical Chemistry 84 (23), 10324-10331.
Hu, C., Yang, D.-P., Zhu, F., Jiang, F., Shen, S., Zhang, J., 2014. Enzyme-labeled Pt@ BSA nanocomposite as a facile electrochemical biosensing interface for sensitive glucose determination. ACS Applied Materials & Interfaces 6 (6), 4170-4178.
Hu, H., Liu, X., Jiang, F., Yao, X., Cui, X., 2010. A novel chemiluminescence assay of organophosphorous pesticide quinalphos residue in vegetable with luminol detection. Chemistry Central Journal 4(1), 1-6.
Le Guével, X., Ho□tzer, B., Jung, G., Hollemeyer, K., Trouillet, V., Schneider, M., 2011. Formation of fluorescent metal (Au, Ag) nanoclusters capped in bovine serum albumin followed by fluorescence and spectroscopy. The Journal of Physical Chemistry C 115(22), 10955-10963.
Lee, J.H., Park, J.Y., Min, K., Cha, H.J., Choi, S.S., Yoo, Y.J., 2010. A novel organophosphorus hydrolase-based biosensor using mesoporous carbons and carbon black for the detection of organophosphate nerve agents. Biosensors and Bioelectronics 25(7), 1566-1570.
Lu, Y., Chen, W., 2012. Sub-nanometre sized metal clusters: from synthetic challenges to the unique property discoveries. Chemical Society Reviews 41(9), 3594-3623.
Mulchandani, P., Mulchandani, A., Kaneva, I., Chen, W., 1999. Biosensor for direct determination of organophosphate nerve agents. 1. Potentiometric enzyme electrode. Biosensors and Bioelectronics 14(1), 77-85.
Qian, S., Lin, H., 2015. Colorimetric sensor array for detection and identification of organophosphorus and carbamate pesticides. Analytical chemistry 87(10), 5395-5400.
Shamsipur, M., Farzin, L., Tabrizi, M.A., Molaabasi, F., 2015. Highly sensitive label free electrochemical detection of VGEF 165 tumor marker based on “signal off” and “signal on” strategies using an anti-VEGF 165 aptamer immobilized BSA-gold nanoclusters/ionic liquid/glassy carbon electrode. Biosensors and Bioelectronics 74, 369-375.
Shamsipur, M., Molaabasi, F., Hosseinkhani, S., Rahmati, F., 2016. Detection of Early Stage Apoptotic Cells Based on Label-Free Cytochrome c Assay Using Bioconjugated Metal Nanoclusters as Fluorescent Probes. Analytical Chemistry 88(4), 2188-2197.
Shang, L., Dong, S., 2008. Silver nanocluster-based fluorescent sensors for sensitive detection of Cu (II). Journal of Materials Chemistry 18(39), 4636-4640.
Shang, L., Dong, S., Nienhaus, G.U., 2011. Ultra-small fluorescent metal nanoclusters: synthesis and biological applications. Nano Today 6(4), 401-418.
Shin, K.-S., Ji, J.H., Hwang, K.S., Jun, S.C., Kang, J.Y., 2016. Sensitivity enhancement of bead-based electrochemical impedance spectroscopy (BEIS) biosensor by electric field-focusing in microwells. Biosensors and Bioelectronics 85, 16-24.

Singh, V.V., 2016. Recent advances in electrochemical sensors for detecting weapons of mass destruction. A Review. Electroanalysis 28, 920-935.
Songa, E.A., Okonkwo, J.O., 2016. Recent approaches to improving selectivity and sensitivity of enzyme-based biosensors for organophosphorus pesticides: A review. Talanta 155, 289-304.
Tang, T., Deng, J., Zhang, M., Shi, G., Zhou, T., 2016. Quantum dot-DNA aptamer conjugates coupled with capillary electrophoresis: a universal strategy for ratiometric detection of organophosphorus pesticides. Talanta 146, 55-61.
Tao, Y., Li, M., Ren, J., Qu, X., 2015. Metal nanoclusters: novel probes for diagnostic and therapeutic applications. Chemical Society Reviews 44(23), 8636-8663.
Tiwari, I., Gupta, M., Pandey, C.M., 2015. Application of Cationic Poly (lactic-co-glycolic acid) Iron Oxide/Chitosan-Based Nanocomposite for the Determination of Paraoxon. ChemElectroChem 2(2), 280-287.
Tiwari, J.N., Nath, K., Kumar, S., Tiwari, R.N., Kemp, K.C., Le, N.H., Youn, D.H., Lee, J.S., Kim, K.S., 2013. Stable platinum nanoclusters on genomic DNA–graphene oxide with a high oxygen reduction reaction activity. Nature communications 4, 2221.
Wang, J., Chow, W., Leung, D., Chang, J., 2012. Application of ultrahigh-performance liquid chromatography and electrospray ionization quadrupole orbitrap high-resolution mass spectrometry for determination of 166 pesticides in fruits and vegetables. Journal of Agricultural and Food Chemistry 60(49), 12088-12104.
Wen, X., Yu, P., Toh, Y.-R., Tang, J., 2013. Quantum confined stark effect in Au8 and Au25 nanoclusters. The Journal of Physical Chemistry C 117(7), 3621-3626.
Xie, J.P., Zheng, Y.G., Ying, J.Y., 2009. Protein-directed synthesis of highly fluorescent gold nanoclusters. Journal of American Chemical Society 131, 888-889.
Xu, Y., Sherwood, J., Qin, Y., Crowley, D., Bonizzoni, M., Bao, Y., 2014. The role of protein characteristics in the formation and fluorescence of Au nanoclusters. Nanoscale 6(3), 1515-1524.
Yang, G., Zhou, Y., Pan, H.-B., Zhu, C., Fu, S., Wai, C.M., Du, D., Zhu, J.-J., Lin, Y., 2016. Ultrasonic-assisted synthesis of Pd–Pt/carbon nanotubes nanocomposites for enhanced electro-oxidation of ethanol and methanol in alkaline medium. Ultrasonics sonochemistry 28, 192-198.
Yu, G., Wu, W., Zhao, Q., Wei, X., Lu, Q., 2015. Efficient immobilization of acetylcholinesterase onto amino functionalized carbon nanotubes for the fabrication of high sensitive organophosphorus pesticides biosensors. Biosensors and Bioelectronics 68, 288-294.
Yuan, D., Chen, S., Yuan, R., Zhang, J., Zhang, W., 2013. An electrogenerated chemiluminescence sensor prepared with a graphene/multiwall carbon nanotube/gold nanocluster hybrid for the determination of phenolic compounds. Analyst 138(20), 6001-6006.
Zhang, S., Li, B., Sheng, Q., Zheng, J., 2016. Electrochemical sensor for sensitive determination of nitrite based on the CuS–MWCNT nanocomposites. Journal of Electroanalytical Chemistry 769, 118-123.
Zhang, T., Zeng, L., Han, L., Li, T., Zheng, C., Wei, M., Liu, A., 2014. Ultrasensitive electrochemical sensor for p-nitrophenyl organophosphates based on ordered mesoporous carbons at low potential without deoxygenization. Analytica Chimica Acta 822, 23-29.
Zhao, H., Ji, X., Wang, B., Wang, N., Li, X., Ni, R., Ren, J., 2015. An ultra-sensitive acetylcholinesterase biosensor based on reduced graphene oxide-Au nanoparticles-β-cyclodextrin/Prussian blue-chitosan nanocomposites for organophosphorus pesticides detection. Biosensors and Bioelectronics 65, 23-30.

Table 1. Comparison of analytical performance of the proposed CuNS-MWCNT modified PGE with previously reported other nanomaterial- modified carbon-based electrodes.

Electrode	Methods	Linear range	LOD	Ref.
OPH Enzyme/MC/CB/GCE	Amperometry	0.2-8 μM	0.12 μM	(Lee et al. 2010)
OPH Enzyme/GO/Nafion/GCE	Amperometry	2-20 μM	0.14 μM	(Choi et al. 2010)
AChE Enzyme/CNT/NH_2/GCE	Amperometry	0.2-30nM	0.08nM	(Yu et al. 2015)
OPH Enzyme/BSA/pH electrode	Potentiometry	150–700 μM	2 μM	(Mulchandani et al. 1999)
Ordered mesoporous carbon/GCE	DPSV	0.01–1and 1-20 μM	1.9 nM	(Zhang et al. 2014)
CuNCs@BSA-SWCNT/GCE	SWV	50–500 nM 0.5-30 μM	12.8 nM	Present work

Table 2. Determination of paraoxon in the water samples (n=3)

Sample	Paraoxon added (μM)	Paraoxon found (μM)	Recovery (%)
River water	0.50	0.45 ± 0.08	95
	2.0	2.1 ± 0.3	93
	10.0	9.8 ± 0.1	97

Waste water	25.0	24.2 ± 0.2	102
	0.50	0.46 ± 0.07	94
	2.0	1.9 ± 0.3	96
	10.0	10.2 ± 0.5	95
	25.0	24.6 ± 0.3	103
Well water	0.50	0.53 ± 0.05	93
	2.0	1.8 ± 0.4	101
	10.0	10.1 ± 0.2	95
	25.0	25.4 ± 0.5	99

Figure captions:

Scheme 1. Schematic representation of biosensor fabrication (a) and suggested mechanism for paraoxon reduction (b).

Figure 1. (a) UV-Vis absorption spectra of free BSA, CuNCs@BSA and CuNCs@BSA-SWCNT nanocomposite, (b) Fluorescence emission spectra of CuNCs@BSA and CuNCs@BSA-SWCNT at λ_{exc}: 325 nm, (c) FT-IR spectra of free BSA, CuNCs@BSA, SWCNT and CuNCs@BSA-SWCNT (D) SEM images of CuNCs@BSA, SWCNT, CuNCs-SWCNT and CuNCs@BSA-SWCNT nanocomposite, respectively and TEM images of CuNCs@BSA.

Figure 2. (a) EIS measurements of bare GCE, CuNCs-SWCNT/GCE and CuNCs@BSA-SWCNT/GCE, (bI) CVs of CuNCs@BSA-SWCNT/GCE in different scan rate, (bII) CVs of GCE, CuNCs-SWCNT/GCE and CuNCs@BSA-SWCNT/GCE in a solution in PBS containing 5 mM $K_4[Fe(CN)_6]^{-4/-3}$ in 1.0 M KCl. (cI) CVs of different modified electrodes in blank and (cII) in the presence of 100 µM paraoxon in PBS (pH = 6.0).

Figure 3. (a) Effect of pH on peak potentials, (b) the SWV response to the reduction of a 10 µM paraoxon in PBS at a CuNCs@BSA-SWCNT/GCE in different pH, preconcentration potential, and preconcentration potential. (c) The SWV in PBS (0.1 M, pH 6.0) containing different concentrations of paraoxon from 0.05 µM to 35 µM, and (d) the corresponding calibration curves.

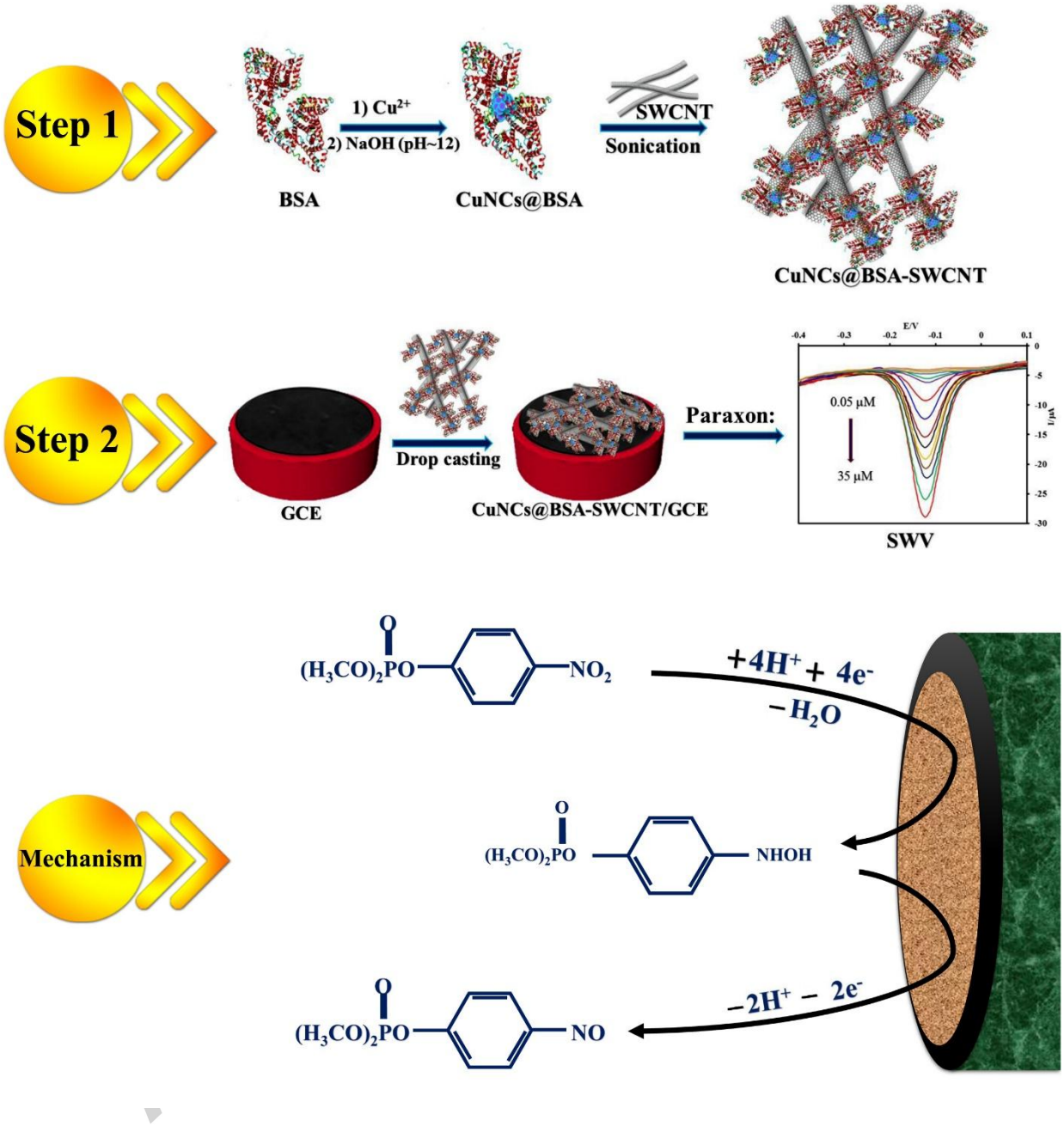
Step 1
1) Cu2+
2) NaOH (pH~12)
BSA
CuNCs@BSA
SWCNT
Sonication
CuNCs@BSA-SWCNT
Step 2
GCE
Drop casting
CuNCs@BSA-SWCNT/GCE
Paraxon:
0.05 μM
35 μM
E/V
SWV
Mechanism
(H3CO)2PO
NO2
+4H+ + 4e-
-H2O
NHOH
NO
-2H+ - 2e-

Scheme 1.

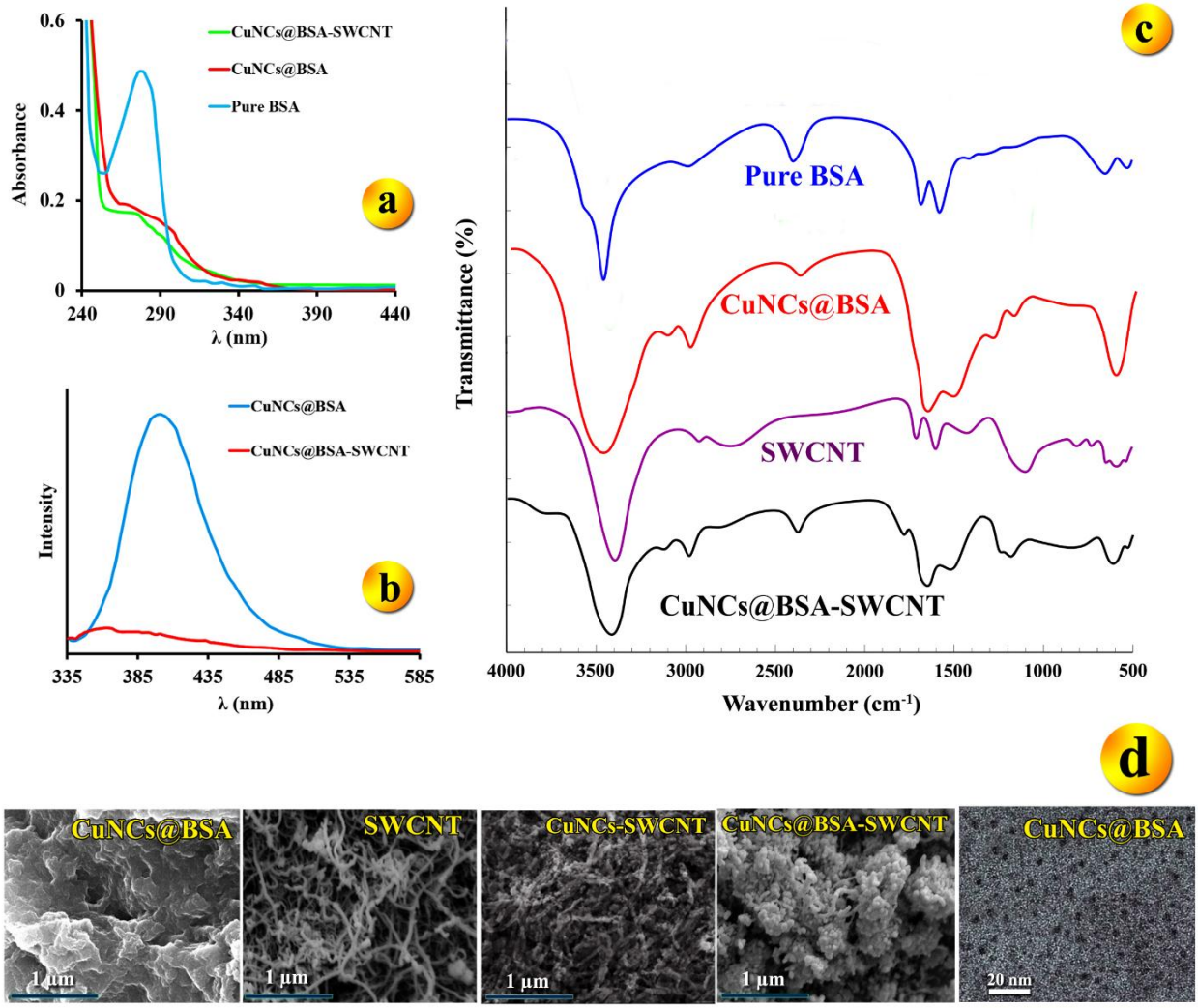

Figure 1

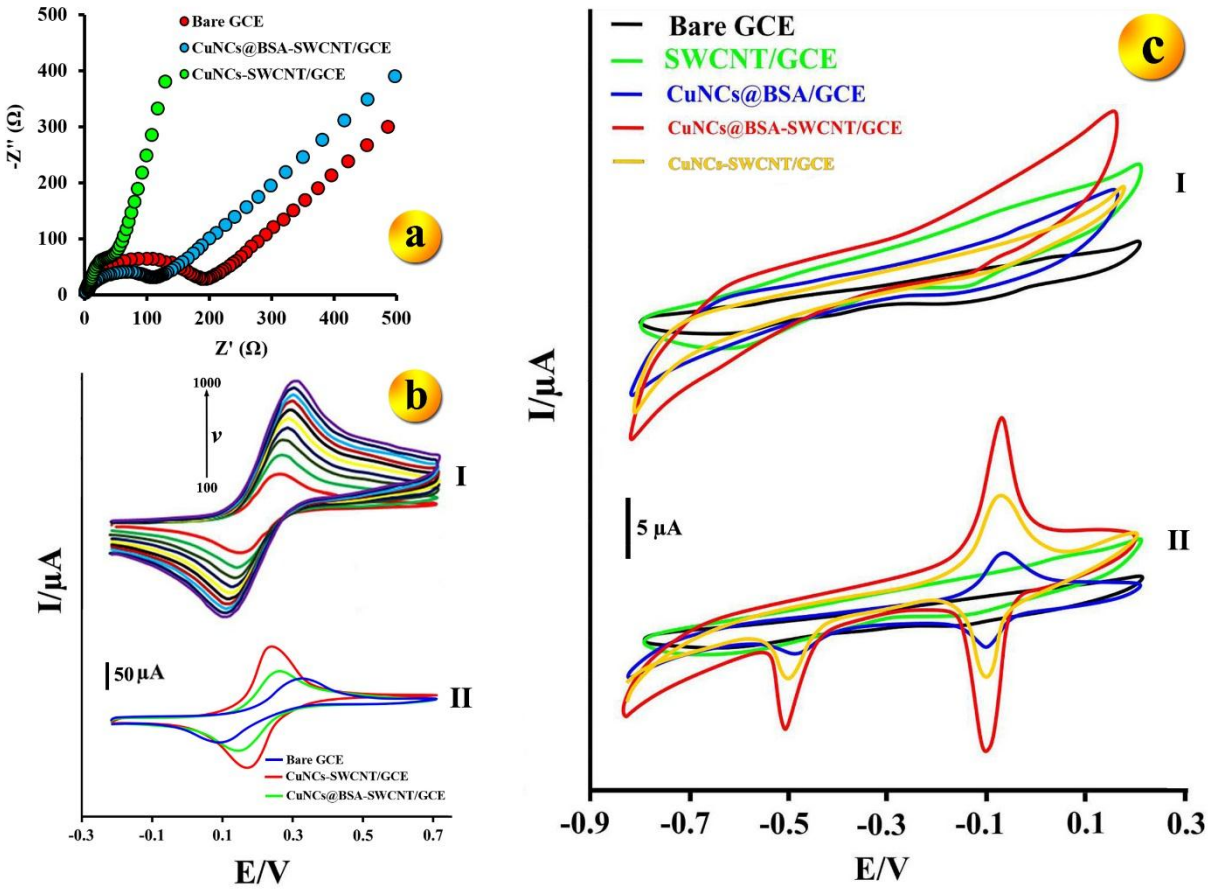

Figure 2

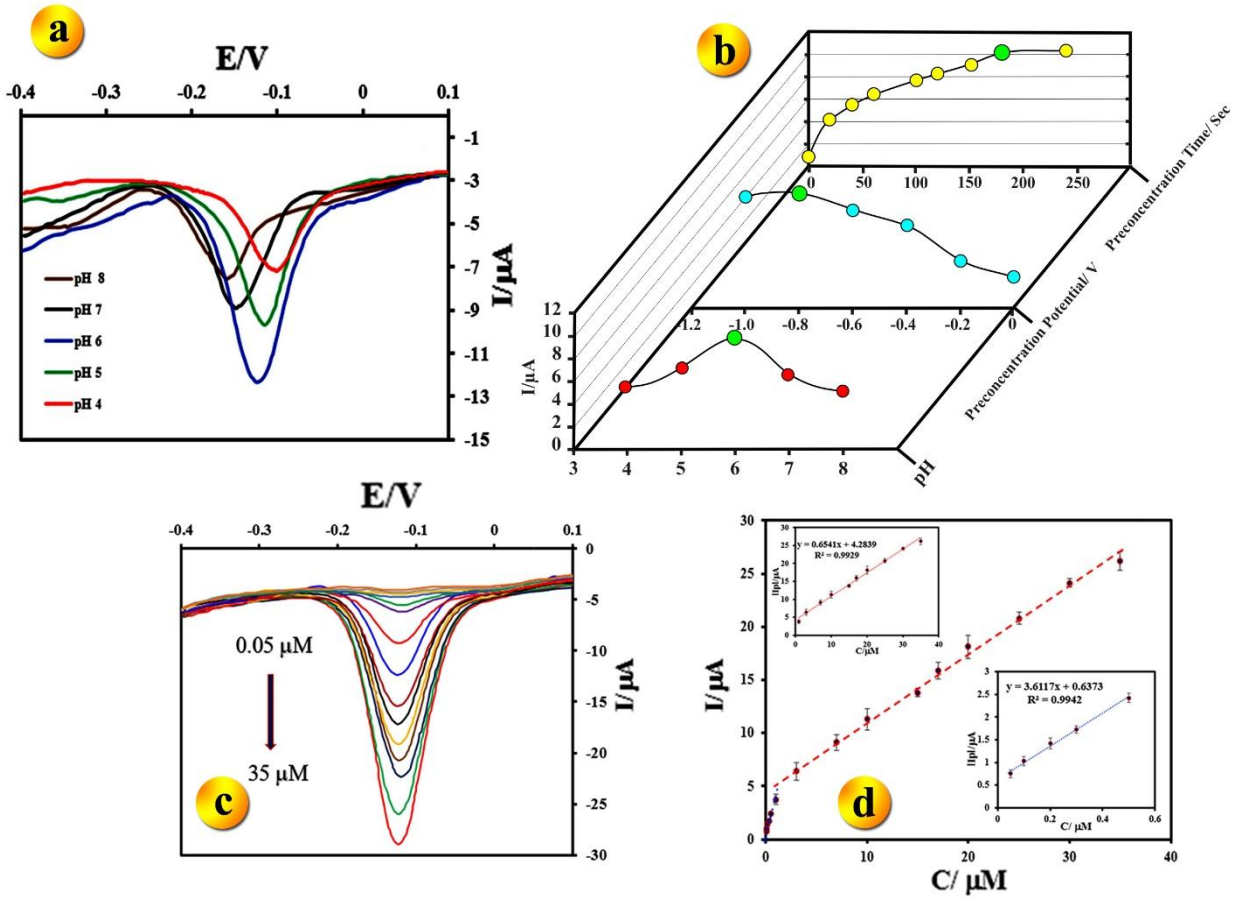

Figure 3

Research highlights

- Nanocomposite of BSA template Cu nanoclusters-SWCNT uses as a novel sensing layer.
- Rapid and direct detection of trace paraoxon using the fabricated enzymeless biosensor.
- High analytical performance of biosensor towards paraoxon reduction was achieved

- The developed sensor was used in real samples with satisfactory results.